Chemistry Africa (2023) 6:2957–2967
https://doi.org/10.1007/s42250-023-00713-4

ORIGINAL ARTICLE

Unveiling 1,3-Thiazine Derivative as a Potential Neuraminidase Inhibitor: Molecular Docking, Molecular Dynamics, ADMET and DFT Studies

Mustapha Abdullahi[1,2] · Adamu Uzairu[1] · Gideon Adamu Shallangwa[1] · Paul Andrew Mamza[1] · Muhammad Tukur Ibrahim[1] · Anshuman Chandra[3] · Vijay Kumar Goel[3]

Received: 18 April 2023 / Accepted: 27 May 2023 / Published online: 22 June 2023

Abstract

The influenza virus is usually influenced by genetic mutations and reassortment of its different strains, resulting in drug resistance and pandemics. This necessitates the search and discovery of more potential influenza inhibitors to prevent future outbreaks. As an extension of our previous report on 1, 3 thiazine derivatives as neuraminidase (NA) inhibitors, compound 4 was selected as the template scaffold for the in-silico drug design due to its better NA inhibitory activity, good binding affinity, and pharmacokinetic profile. Therefore, a newly designed 4a compound resulted in better binding affinity (MolDock score) in comparison with the template scaffold and the oseltamivir as the reference drug. The conformational stability of the compound in the binding cavity of the targeted NA protein (3TI6) revealed hydrogen bondings and water-mediated hydrophobic interactions with the active residues after the system stabilized at 100 ns of molecular dynamic (MD) simulation. The drug-likeness and ADMET prediction of the designed 4a revealed non-violation of Lipinski's rule with good pharmacokinetic properties. In addition, the DFT calculations portrayed the relevance of the compound in terms of chemical reactivity due to its smaller band energy gap. The outcome of this study proposed a reliable in-silico perspective for anti-influenza drug discovery and development.

Keywords Influenza · MolDock score · Neuraminidase · Binding cavity · Residual interaction

Abbreviations

COVID-19	Coronavirus2019 disease
NA	Neuraminidase
HA	Hemagglutinin
MD	Molecular dynamics
ADMET	Absorption distribution metabolism excretion and toxicity
SARS-CoV-2	Severe acute respirasyndrome coronavirus 2
WHO	World Health Organization
IAV	Influenza A virus
A(H1N1)pdm09	H1N1 subtype of 2009 influenza pandemic
MVD	Molegro virtual docker
PLP	Piecewise linear potential

✉ Mustapha Abdullahi
mustychem19@gmail.com

Adamu Uzairu
adamuuzairu@yahoo.com

Gideon Adamu Shallangwa
gashallangwa@gmail.com

Paul Andrew Mamza
paulmamza@yahoo.com

Muhammad Tukur Ibrahim
muhdtk1988@gmail.com

Anshuman Chandra
anshuman.chandra2007@gmail.com

Vijay Kumar Goel
vkgoel14@gmail.com

[1] Faculty of Physical Sciences, Department of Chemistry, Ahmadu Bello University, P.M.B. 1044, Zaria, Kaduna State, Nigeria

[2] Faculty of Sciences, Department of Pure and Applied Chemistry, Kaduna State University, Tafawa-Balewa Way, Kaduna, Kaduna State, Nigeria

[3] School of Physical Science, Jawaharlal Nehru University, New Delhi 110067, Delhi, India

RMSD	Root mean squaredeviation
NPT	Normal pressure and temperature
FMO	Frontier molecular orbital
E-LUMO	Lowest unoccupied molecular orbital energy
E-HOMO	Highest occupied molecular orbital energy
SID	Simulation interaction diagram
RMSF	Root mean square fluctuation
MEP	Molecular electrostatic potential

1 Introduction

Since emerging influenza may cause a global pandemic, it remains a danger to public health [1]. The influenza virus is a member of the Orthomyxoviridae family, which is responsible for a high rate of illness and death in people worldwide [2]. The four primary kinds of influenza viruses are designated as A, B, C, and D, with A and B causing seasonal influenza epidemics [3]. The influenza A virus (IAV) has largely been documented to infect humans, and it is classified into subtypes based on the protein reassortments on the viral surface [4]. The 2009 pandemic was caused by the H1N1 subtype of IAV, which is generally referred to as A(H1N1)pdm09 and has progressively supplanted the seasonal influenza A(H1N1) virus [5]. As a result, only type A viruses have been linked to influenza pandemics. Prior to 2020, the influenza virus was believed to be one of the most common non-COVID-19 respiratory viruses [5, 6]. Nevertheless, the virus's circulation decreased significantly during the first wave of the COVID-19 pandemic in 2020 [7]. Even though many localities have a high prevalence of COVID-19 infections, most nations reported intermittent influenza detections to the World Health Organization (WHO) [8]. Throughout the SARS-CoV-2 pandemic, there has been a 99% decrease in influenza virus isolation globally [9]. Influenza may return and spread after the SARS-CoV-2 pandemic [9]. According to WHO prevalence figures, there are around 2–5 million cases of severe influenza infections worldwide, with over 500,000 fatalities [10].

The currently circulating IAV subtypes in humans are H1N1 and H3N2, and hemagglutinin (HA) and neuraminidase (NA) are the two essential transmembrane glycoproteins found on the surface of the influenza virus [11]. The NA has three main functions: it aids the virus access to epithelial cells by breaking down respiratory tract mucins rich in sialic acids; it desialylated the virion and the cytoplasmic membrane, maximizing the fusogenic potential of the HA; and it promotes the production of new virions and prevents their accumulation on the surface of the host cell [12]. Because of the highly conserved binding site in the NA protein structure, it is an attractive molecular target for the discovery of new influenza virus inhibitors [13]. The basic and acidic groups found in the catalytic cavity of the NA-targeted protein are the two critical active pharmacophores of NA inhibitors [14]. The majority of the FDA-approved NA inhibitors, such as zanamivir (RelenzaTM) and oseltamivir (TamifluTM) are licensed for influenza treatment in several countries [15]. The rapid spreading of new influenza strains is becoming resistant to conventional vaccinations and drugs for treatment and protection respectively [16]. In addition, the emergence of drug-resistant strains of the influenza virus is due to the genetic mutability and resortments which has attracted the interest of many experts [15]. This necessitates the search quest for more powerful NA inhibitors. Yet, the experimental trial-and-error technique used in drug discovery and development is tedious, time-consuming, and labor-intensive [17]. These constraints have been seen to be addressed by the use of theoretical models and computational techniques. The use of computer-aided drug design (CADD) gives knowledge and understanding of a technique that can provide important information about the kinds of interaction and binding affinity between protein and ligand (complex) [18]. One of the most popular methods is molecular docking, which predicts possible drug binding modes at a particular target-binding site and measures affinity based on the drug's conformation and complementarity with the characteristics found in the binding pocket [19]. Furthermore, the structure-based drug design (SBDD) method relies on the availability and understanding of the targeted receptor to build compounds with greater binding efficiency [20]. The molecular dynamics (MD) simulations estimate how the atoms in a protein or other molecular system move over time based on the fundamental physics model (Newtonian motion) [21]. Also, when evaluating potential medicine candidates for safety and effectiveness, the characteristics of absorption, distribution, metabolism, elimination, and toxicity (ADMET) are crucial [22]. To prevent drug rejections in later stages of clinical trials, ADMET prediction needs to be implemented.

Compound 4 (1 g) has been reported to have the best NA inhibitory rate of 68.08% (29.06 µg/mL) with good binding potentials and can be used as a template for the future design of potential candidates in previous studies [23, 24]. As a result, the current research employs this most active compound as a template scaffold to design a potent analog via a structure-based design strategy. In addition, the binding affinity and molecular dynamic stability of the targeted NA receptor are studied. The pharmacokinetics and frontier molecular orbital simulations of the designed analog are investigated to provide a molecular understanding of its chemical reactivity and potency.

2 Materials and Methods

2.1 Template Scaffold Selection and Modification Strategy

Compound 4 (ethyl 2-acetamido-4-methyl-6-(2-(pentan-3-yloxy)phenyl)-6 H-1,3-thiazine-5-carboxylate) of our previous report [24], was utilized as the template scaffold for the structural modification. The basis for this selection was because the compound has the; (i) highest NA activity, (ii) high binding affinity, (iii) favourable pharmacokinetic profile, and (iv) within the chemical space of our developed QSAR models [24]. The modification was done near the (pentan-3-yloxy) benzene fragment of the template with a steric and electronegative moieties in line with our QSAR modelling and molecular docking studies. Thus, the ethyl 2-acetamido-6-(6-acetamido-5-amino-3-ethoxy-5,6-dihydronaphthalen-2-yl)-4-methyl-6 H-1,3-thiazine-5-carboxylate was obtained as the modified compound (designed 4a) for further in-silico studies. Figure 1 shows the modification scheme of the template 4 to the designed 4a compounds.

2.2 Preparation of Ligand and Target Protein Receptor for Molecular Docking Analysis

The 2D structures of the compounds were drawn using Chem Draw software and then optimized using Spartan 14 software at the density functional level of theory (DFT) with Becke three-parameter hybrid exchange potentials of Lee-Yang-Parr correlation potential (B3LYP) and 6-31G* basis set [25, 26]. The NA target of A/California/04/2009 (H1N1) strain complexed with oseltamivir (PDB code: 3TI6) was retrieved from the protein data bank at www.rcsb.org/pdb, which is a repository for the 3D crystal structures of large biomolecules. NA proteins are commonly selected due to the observation of the open conformation for the 150-loop in the N1 and N8 (group 1 structures) which shows intrinsically lower energy than the closed-loop conformation for these enzymes [27]. The group 1 structures of the neuraminidase bind to oseltamivir in this open conformation but later switch to the closed conformation. Hence, it appears that the binding of oseltamivir towards group-1 neuraminidases prefers the closed conformation of the 150-loop (higher energy) that it possibly accesses through a relatively slow conformation change [27]. Thus, it should be possible to develop novel inhibitors for group 1 neuraminidase that is selective for the open 150-loop conformation with the ability to bind more strongly than oseltamivir [27]. The studied compounds were docked with the NA target to review their binding affinities using Molegro Virtual Docker (MVD) [28, 29]. The MVD was initially used to identify potential binding cavities/active sites for the target protein of interest. However, several binding cavities were predicted but only one was selected in view of the existing knowledge about the active residues in the literatures [30, 31]. The selected optimum active cavity was further used in our subsequent docking and molecular simulation investigations. The cavity was set within a constraint sphere of 15 Å radius with the center coordinate of X: − 28.02, Y: 14.69, Z: 20.22 for the docking simulation as shown in Fig. 2. The MolDock (Grid) score at a default grid resolution of 0.3 Å was set up for 10

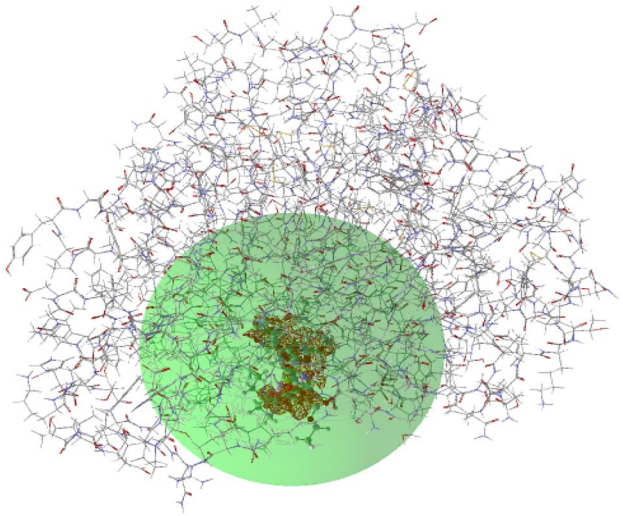

Fig. 2 Optimum detected binding cavities for the NA targets, volume: 92.672 $Å^3$, surface area: 247.04 $Å^2$ for PDB: 3TI6 at radius 15

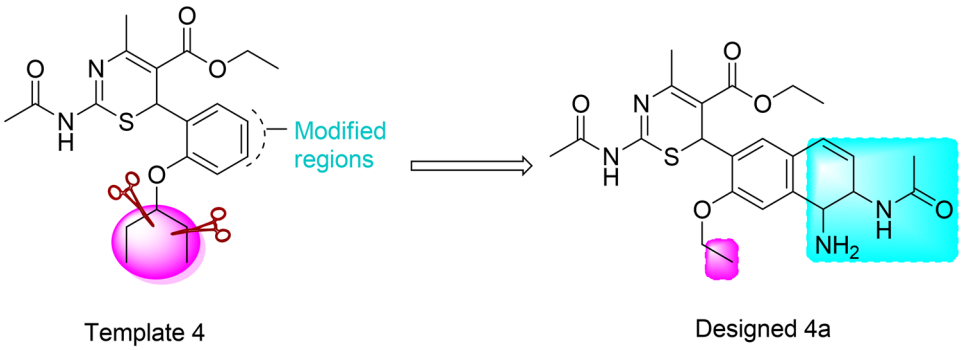

Fig. 1 2D structures of the template scaffold (compound 4) and the newly designed compound (designed 4a) showing the modified regions in purple, and cyan colour

independent runs, and each run with a maximum number of 1500 iterations on a single population size of 50. The detailed steps for the MVD docking procedure and scoring functions have been described in our previous articles [29, 32].

2.3 Molecular Dynamics Study

To explore the binding stability of the lead molecule in the most stable complex formed, the Molecular Dynamics(MD) simulation study was carried out using the Desmond MD program on Ubuntu 18.04 of an HP computer workstation (Z2 G2 TOWER) having NVIDIA Quadro 6000, graphics processing unit (GPU) of 4GB, and OPLS-3e force field [33, 34]. The best ligand-protein complex acquired was loaded to the interface of Maestro of the Schrodinger software which was located at the center of the orthorhombic box shape (with size as 10 Å × 10 Å distance). To solvate, the simulation box, single-point charge (SPC) water molecules were added with appropriate counter ions to neutralize the system [35, 36]. The 0.15 M NaCl salt concentration was set to mimic the physiological conditions using the Desmond System Builder panel. Using the OPLS3e force field, the energy of the overall system was minimized with 2000 iterations and a convergence criterion of 1 kcal/mol to remove electronic conflict between protein structures [37, 38]. The production MD simulation was run for 1000 steps for 100 ns at 298 K and 1 bar using the NPT (Normal pressure and temperature) ensemble. The Nose-Hoover Chain thermostat algorithm and Matrtyna–Tobias–Klein barostat algorithm were used to uphold temperature and pressure during the simulation [39, 40]. The dynamic behavior and interactions between designed 4a and the NA target (3TI6) were analyzed using the Simulation Interaction Diagram (SID) tool, where the *out.cms* file was loaded and selected for the Root Mean Square Deviation (RMSD) and Root Mean Square Fluctuation (RMSF) analysis.

2.4 Lipinski's Rule and ADMET Characteristics Prediction

The preliminary evaluation of ADMET/pharmacokinetic features of potential drug candidates is vital at the early stage of drug development [41]. Therefore, an effective and precise pkCSM website was utilized to predict a variety of pharmacokinetic characteristics, as well as the drug-likeness and toxicity assessments of the proposed compounds in the study.

2.5 Density Functional Theory Calculations

The Density Functional Theory (DFT) analysis is an important computational approach for studying the electronic structure, stability, and reactivity of compounds based on some relevant quantum chemical descriptors computed from the frontier molecular orbital (FMO) energies such as the lowest unoccupied molecular orbital energy (E_{LUMO}) and the highest occupied molecular orbital energy [42]. In this study, the quantum-chemical descriptors of the compounds were generated to examine their chemical reactivity. These descriptors include Ionization potential ($IP = -E_{HOMO}$), Electron affinity ($EA = -E_{LUMO}$) index, Energy gap ($\Delta E = E_{LUMO} - E_{HOMO}$), Electronegativity ($\chi = -(E_{LUMO} + E_{HOMO})/2$), Chemical hardness ($\eta = (E_{LUMO} - E_{HOMO})/2$), and Chemical softness ($S = 1/\eta$) [43]. In addition, the molecular electrostatic potential (MEP) surfaces were also computed from the population analysis. These are important parameters used in elucidating the efficiency of compound interaction in the binding site of the NA target enzyme.

3 Results and Discussion

3.1 Molecular Docking Studies

The binding cavity of all NA targets of influenza consists of 3 active residues arginine (Arg 118, Arg 292, and Arg 371) which bind the carboxylate moiety of the sialic acid substrate, the acetamido moiety interacts with Arg 152 while the 8- and 9-hydroxyl groups of the substrate forms H-bonds with Glu 276 residue [44]. The predicted binding cavity with their amino acid residues by MVD and supported by numerous literatures is shown in Fig. 3.

The validation of the docking algorithm is an essential step to ensure that ligand molecules bind within the active cavity of the receptor in a precise conformation through the

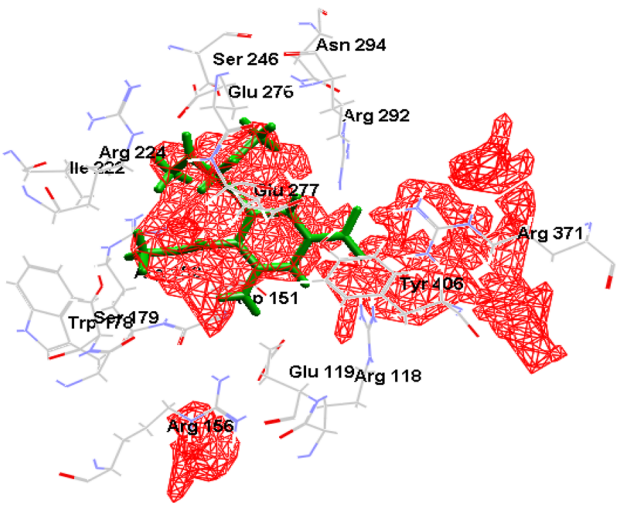

Fig. 3 Predicted binding cavities of the NA target (PDB: 3TI6) by MVD and their active residues

accurate selection of size and center coordinates of the grid box [45]. As such, the docking simulation protocol was validated by redocking the co-crystalized structure of the NA target with oseltamivir using the MolDock Simplex Evolution (MolDock SE) search algorithm. The best binding pose parameters of the studied molecules were reported as MolDock (kcal/mol), re-rank, RMSD, and H-bond energies in Table 1.

The various binding poses obtained are similar to the co-crystalized ligand, and the RMSD scores are less than 2 Å. The RMSD of the best binding pose of oseltamivir was 1.12 Å, with a MolDock score of − 144.85 kcal/mol and H-bond energy of − 9.68 kcal/mol which is similar to the results obtained for the docked conformer and co-crystallized NA target (PDB:2HU0) with oseltamivir[27]. However, the oseltamivir binds to the active cavity of the NA target (3TI6) through H-bond interactions with Arg 118, Arg 292, Glu 119, and Arg 371 amino acid residues as elucidated in Fig. 4. Others are Arg 118, Glu 277, Arg 292, and Arg 371 for electrostatics interactions while Arg 118, Asp 151, Glu 119, Glu 277, Arg 292, and Arg 371 for steric interactions.

The RMSD score of the best binding pose of template 4 was 6.13 Å, with a MolDock score of − 137.05 kcal/mol and H-bond energy of − 2.23 kcal/mol. The template 4 compound majorly formed one H-bond interaction with Arg 371 residue (Fig. 5) while Arg, 118, Arg 371, Trp 403, Ser 404,

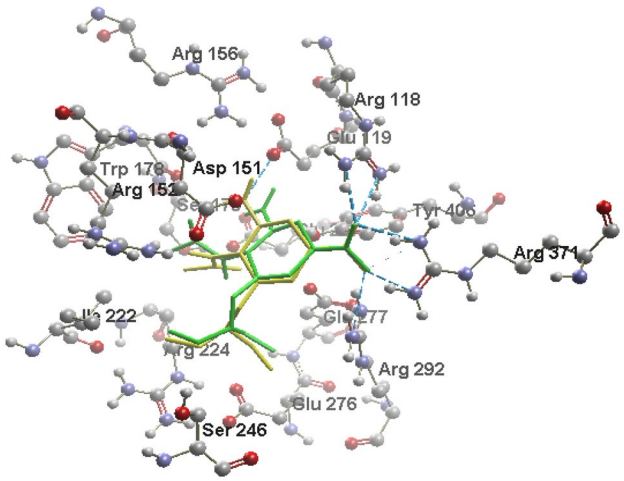

Fig. 4 Best binding pose (yellow) and the co-crystallized NA target (PDB: 3TI6) with Oseltamivir (green)

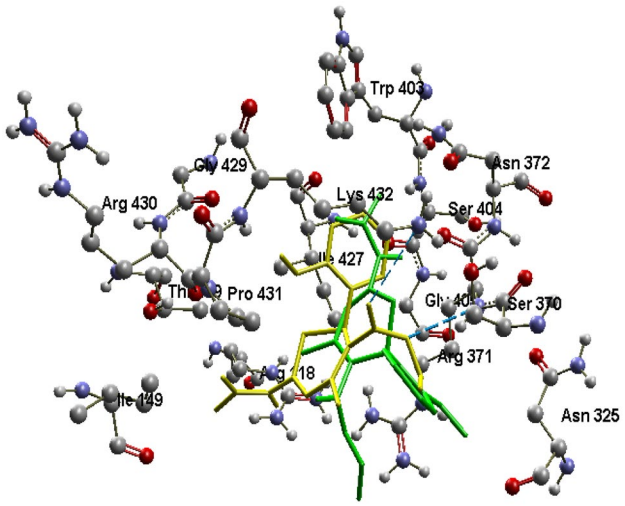

Fig. 5 Best binding pose (yellow) and the co-crystallized NA target (PDB: 3TI6) with template 4 (green)

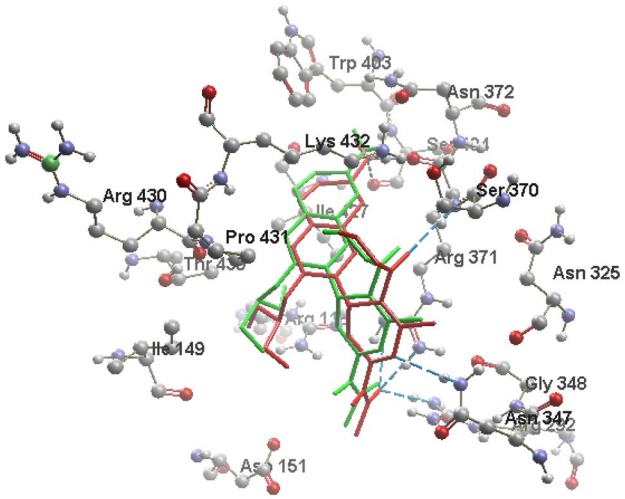

Fig. 6 Best binding pose (yellow) and the co-crystallized NA target (PDB: 3TI6) with designed 4a (red)

Table 1 MolDock (kcal/mol), Rerank, RMSD and H-bond energy scores of the studied molecules with NA target (3TI6)

Ligand	MolDock score (kcal/mol)	Rerank score	RMSD (Å)	HBond
[00][00]4a	− 159.22	− 103.06	0.86	− 12.74
[00][00]Oseltamivir	− 144.85	− 109.36	1.13	− 9.69
[00][00]4	− 137.05	− 90.52	6.13	− 2.23

Pro 431, Lys 432, and Ile 427 interact through steric interactions. However, the lowest RMSD score of 0.86 Å was recorded for the best binding pose of the newly designed 4a, with the highest MolDock score of − 159.22 kcal/mol and highest H-bond energy of −12.72 kcal/mol. This implies that the designed 4a binds more efficiently with the active residues of the NA target (complex 4a) through H-bond interactions with Arg 292, Arg 371, Asn 347, and Ser 404 amino acids as shown in Fig. 6. Complex 4a also formed more steric interactions with Asp 151, Tyr 406, Asn 347, Arg 371, Arg 292, Ser 369, Thr 439, Ile 427, Asn 325, and Pro 431 residues. Therefore, complex 4a with the highest MolDock and H-bond energy scores was selected for further residual and conformational stability analysis through MD simulations.

3.2 MD Simulation Study

The conformational stability of the bound conformation for designed 4**a** in the binding cavity of the targeted NA protein (PDB: 3TI6) was studied via MD simulation. The studied complex 4a system was simulated for up to 100 ns which is enough for the Cα atoms configurations. Both RMSD and RMSF plots were generated at the end of the 100 ns simulation period. Thus, the RMSD analysis shows the general overview of the conformational stability of the complex during the simulation period. Lower RMSD scores during the simulation interval are related to the stable conformation of the protein-ligand complex and vice versa [46–50]. More so, significant RMSD fluctuations suggest a substantial conformational change of the targeted protein during the simulation while smaller fluctuations are acceptable for negligible conformational changes.

The RMSD plot of complex 4a was presented in Fig. 7A, and it was observed that the RMSD of the protein and ligand 4a negligibly fluctuates within the permissible range of 1–2.2 Å throughout the MD trajectory of 100 ns. Since the RMSD plots of the protein backbone and ligand 4a were lying over each other during the simulation interval, a stable bound conformation of complex 4a can be inferred. The binding efficiency of ligand 4a was also studied using the RMSF values for all alpha-carbon atoms of all amino acid residues of the targeted protein based on the MD trajectory of 100 ns as shown in Fig. 7B. The RMSF defines the average deviation from the original site for each protein residue which depicts its flexibility and mobility throughout the simulation period [51]. Hence, high RMSF values suggest high backbone flexibility, while small RMSF values suggest good backbone stability during the simulation. In this plot, insignificant fluctuations

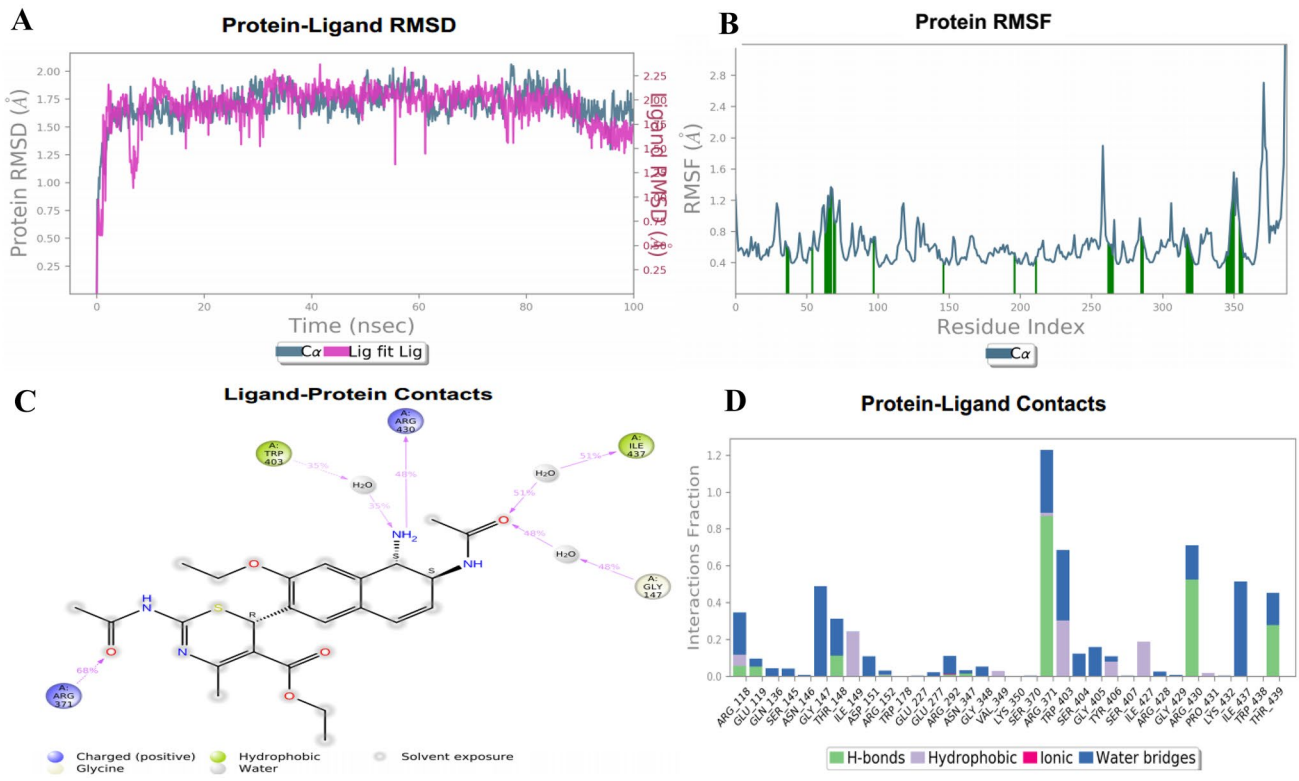

Fig. 7 MD simulation analysis of complex 4a, **A** RMSD (Protein RMSD in grey colour while RMSD of ligand 4**a** in red), **B** Protein RMSF plot, **C** 2D Interaction diagram, and **D** Protein-ligand contact analysis

(below 2.0 Å) during the interactions were observed which is an indication of a minimal conformation change and perfectly acceptable. This implies that the studied ligand 4a was tightly bound within the binding cavity of the NA binding pocket. The active residues of the targeted NA protein contributing to the interactions with ligand 4a were Arg 371, Ile 437, Arg 430, Gly 147, and Trp 403, with percent contributions of 68%, 51%, 48%, 48%, and 35%, respectively (Fig. 7C). Thus, ligand 4a binds the active residues through hydrogen bonding and water-mediated hydrophobic interactions after the simulation, as shown in Fig. 7D.

3.3 Lipinski's Drug-likeness Rule and ADMET Prediction

For the purpose of avoiding the tendency of a failed drug candidate, the designed 4a was subjected to drug-likeness and ADMET appraisals as mentioned previously [52, 53]. Lipinski's rule was utilized to appraise the drug-likeness properties of the compounds. The rule suggests that a drug-like molecule should not violate more than two of the following criteria which include; MW ≤ 500 g/mol (molecular weight), Log P ≤ 5 (n-octanol/water distribution coefficient), nHA ≤ 10 (number of hydrogen bond acceptors), and nHD ≤ 5 (number of hydrogen bond donors) [54–56]. Interestingly, ligand 4a showed non-violation of Lipinski's rule and was compared with template 4 as shown in Table 2, and its synthetic accessibility (SA) score of 5.63 is within the average range as compared with template 4. This suggests that the studied molecule would be easily synthesized.

The percent absorbance of less than 30% depicts low human intestinal absorption, but the designed 4a was predicted to have 74.18%, which is comparable with the 67.88% of oseltamivir and the 86.31% of template 4. This indicates the ease of absorption of the studied compound in the human intestine. The volume of distribution at a stable state (VDss) depicts an effective distribution of drug candidates to the tissues at sufficient time. A VDss score of greater than 0.5 signifies that the candidate tends to spread in the plasma, while a VDss score of below − 0.5 suggests that the drug has a low tendency to spread to the cell membrane. As such, the VDss scores of the studied compounds 4, 4a, and oseltamivir are predicted as 0.047, − 0.098, and − 0.154 respectively which suggest proper distribution in the plasma. The metabolism in the body is an enzymatic process that helps in drug biotransformation due to the production of numerous metabolites that are crucial in catalyzing the biochemical reaction with different drug concentrations [57–59]. The cytochrome P450 enzyme plays a vital role in the metabolic process of the drug molecules. Out of the 57 cytochrome P (CYP) genes from 17 families were identified in humans. More so, only CYP1, CYP2, CYP3, and CYP4 are utilized in drug metabolism, with CYP (1A2, 2C9, 2C19, 2D6, and 3A4) in charge of the biochemical transformation of more

Table 2 Lipinski's rule and synthetic accessibility score of the designed molecules

Sr No.	MW (g/mol)	Log P	nHA	nHD	nLV	Synthetic accessibility
Rule	≤ 500	≤ 5	≤ 10	≤ 5	≤ 2	–
4	486.58	2.06	7	3	0	5.63
4a	473.59	3.27	6	2	0	5.37
Comment	Passed	Passed	Passed	Passed	Passed	Passed

Table 3 ADMET parameters of the newly designed molecules

Comp. No.	Absorption	Distribution	Metabolism							Excretion	Toxicity
	Intestinal absorption (human) (%)	VDss (human) (Log L/kg)	Substrate and inhibitors of CYP							Total clearance	AMES
			CYP Substrate		CYP inhibitors						
			2D6	3A4	1A2	2C19	2C9	2D6	3A4		
4	86.31	0.047	No	Yes	No	No	No	No	Yes	0.45	No
4a	74.18	− 0.098	No	Yes	No	No	No	No	Yes	0.22	No
Oseltamivir	67.88	− 0.154	No	No	No	No	No	No	No	0.92	No

Table 4 Quantum chemical descriptors of the designed molecules

Molecules	E-HOMO (eV)	E-LUMO (eV)	ΔE (eV)	IP (eV)	EA (eV)	χ (eV)	η (eV)	S (eV)
Template 4	− 6.43	− 2.54	3.89	6.43	2.54	4.49	1.95	0.51
Designed 4a	− 5.78	− 2.57	3.21	5.78	2.57	4.18	1.61	0.62

than 90% of drugs experiencing metabolic processes in phase I. Both template 4 and designed 4a were predicted to be inhibitors and substrates of CYP3A4 only, while the oseltamivir was predicted as a non-substrate/inhibitor. The total clearance level is a measure that defines the correlation between the rate of drug elimination and its concentration in the body. A low clearance score infers high drug endurance in the body, and it was observed that the studied compounds showed low scores. Besides, it is essential to inspect whether the predicted molecules are non-toxic in the cause of drug selection. Interestingly, designed 4a of the study was predicted as non-toxic as shown in Table 3.

3.4 DFT Studies

The frontier molecular orbital energies are important quantum descriptors that explain some key features of molecules relating to charge transfer and interactions at the binding site of the targeted enzyme [36]. The quantum descriptors for the studied compounds were generated from the DFT calculations as earlier stated (Table 4**).** The energy difference between LUMO and HOMO is referred to as the energy gap/band gap which describes the chemical reactivity of the molecules [60–62]. In addition, a smaller energy gap usually has a substantial effect on the intermolecular charge transfer and biological activity of molecules while a large energy gap negatively affects the electrons moving from the HOMO to LUMO, thereby causing weak affinity of the molecule towards the protein enzyme [63, 64].

The higher E-HOMO values of the studied compounds are − 6.43 eV and − 5.78 eV for template 4 and designed 4a respectively, which shows the tendency of these molecules to donate electrons to a suitable molecule with lower energy or empty molecular orbital [65]. Also, the lower E-LUMO are − 2.54 eV and − 1.57 eV for template 4 and designed 4a respectively, which depicts the ability of these compounds to accept electrons. The smaller energy gap (ΔE) is an indication of better chemical stability for complex formation. Hence, the chemical reactivity of the molecules increases with a decrease in the energy gap between HOMO and LUMO energies [66].

The chemical hardness (**η**) of a molecule is also interrelated to its chemical reactivity and stability [67]. Hard molecules tend to have a large energy gap between HOMO and LUMO, which indicates less chemical reactivity while a smaller energy gap depicts a softer and more stable molecule [68]. The quantum descriptors for the designed 4a having the best binding

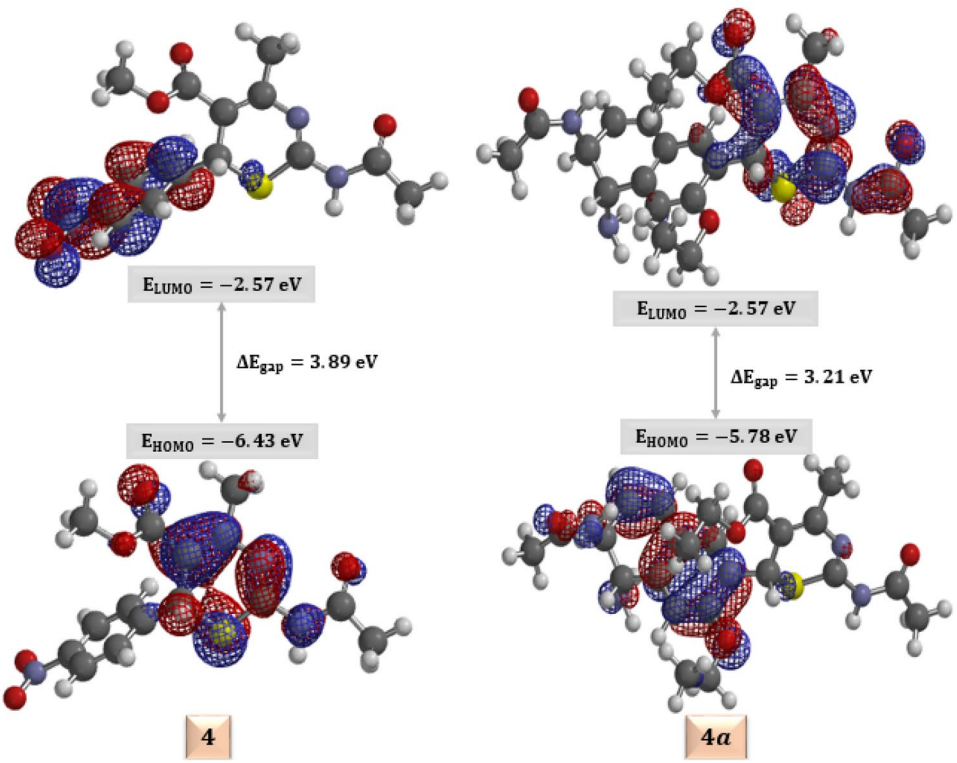

Fig. 8 LUMO-HOMO mesh surface diagram of template 4 and designed 4a at B3LYP/6-31G* basis set of DFT geometrical optimization in vacuum

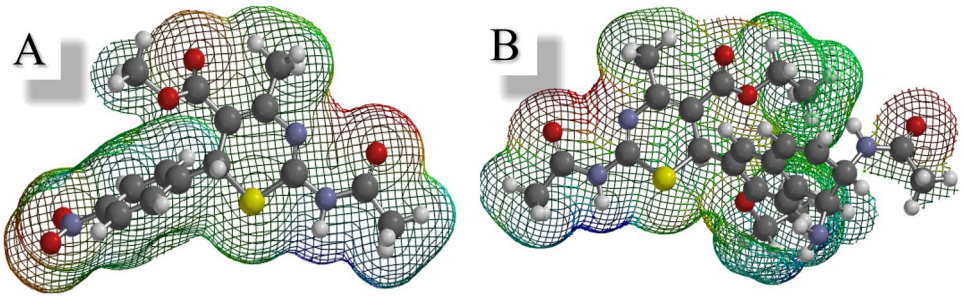

Fig. 9 MEP mesh surface distribution of the optimized structures, **A** template 4, **B** designed 4a, (Blue mesh = positive potential regions, red = negative potential regions, green = zero potential regions)

pose with PDB: **3TI6** receptor was computed as ΔE (3.21 eV), IP (5.78 eV), EA (2.57 eV), χ (4.18 eV), η (1.61 eV), and S (0.62 eV). Furthermore, the band gap of the designed compound was observed to be slightly smaller than the template. This could also support the assertion on the relevance of the designed 4a as a better inhibitor toward the NA target. The HOMO and LUMO mesh surface of the optimized structure of 4a in comparison with the template at DFT/B_3LYP/6-31G* calculations were presented in Fig. 8.

The surface charge distribution can be described by the molecular electrostatic potential map (MEP) of a compound, which provides a good understanding of its physical and chemical properties [42]. The MEP of a molecule predicts the electrophilic and nucleophile centers. Figure 9 elucidates the mesh MEP surfaces around the studied ligands; the red mesh colour represents the nucleophilic area, the blue mesh colour represents the electrophilic zone, and the green mesh colour represents the zero potential zone. In most scenarios, the negative potentials (red mesh) are sited on the O-atoms, while the positive potentials (blue mesh) are close to H-atoms, and the green mesh (neutral potential) are embedded on the C-atoms of the ligands [42, 69]. However, the various positive and negative centers of the studied molecules are important in forming the residual interactions in protein-ligand complexes.

4 Conclusion

In conclusion, the in-silico study unveiled "ethyl 2-acetamido-6-(6-acetamido-5-amino-3-ethoxy-5,6-dihydronaphthalen-2-yl)-4-methyl-6H-1,3-thiazine-5-carboxylate" (designed 4a) as potential NA target through an in-silico designing strategy. The designed 4a showed a better MolDock score of − 159.22 kcal/mol when docked with PDB: 3TI6 receptor and compared with the template 4 and the oseltamivir drug. The binding ability of designed 4a to remain tightly bound with numerous active residues and 430 loop cavities in the binding site of the targeted NA protein was further confirmed through MD simulation for 100 ns. The compound was predicted to be bioavailable with drug-like properties by not violating Lipinski's drug-likeness rules. Thus, the designed 4a was predicted to have a good pharmacokinetic and non-toxicity profile with a smaller energy gap. Therefore, the outcome of this study could serve as a course for the design and synthesis of novel NA inhibitors for influenza therapy.

Acknowledgements The authors remain grateful to the G.F.S. Harrison Quantum Chemistry Research Group in the Department of Chemistry, Ahmadu Bello University, Zaria.

Author Contributions MA, AU, GAS, PAM, and MTI did the conception and design of the work. MA, MTI, did the acquisition and analysis of the data. MA and MTI interpreted the data. MA, and MTI, drafted the manuscript. AC handled the MD simulation protocol, and VKG analyzed the MD simulation results. All authors read and approved the final manuscript.

Funding None.

Declarations

Conflict of interest The authors declare no conflict of interest.

References

1. Prosperi S, Chiarelli F (2022) COVID-19 and diabetes in children. Ann Pediatr Endocrinol Metab 27(3):157–168
2. Pourmomen M, Younesian O, Hosseinzadeh S, Hosseini Alarzi SS, Pourmomen M, Joshaghani H (2023) Frequency of influenza infection in symptomatic patients suspected of having COVID-19. Iran J Med Microbiol 17(1):112–116
3. Feng Q, Huang X-Y, Feng Y-M, Sun L-j, Sun J-Y, Li Y et al (2022) Identification and analysis of B cell epitopes of hemagglutinin of H1N1 influenza virus. Arch Microbiol 204(9):594
4. Kandeil A, Kayed A, Moatasim Y, Aboulhoda BE, El Taweel AN, Kutkat O et al (2023) Molecular identification and virological characteristics of highly pathogenic avian influenza A/H5N5 virus in wild birds in Egypt. Microb Pathog 174:105928
5. Li J, Zhang Y, Zhang X, Liu L (2022) Influenza and Universal Vaccine Research in China. Viruses 15(1):116
6. Chow EJ, Uyeki TM, Chu HY (2022) The effects of the COVID-19 pandemic on community respiratory virus activity. Nat Rev Microbiol. https://doi.org/10.1038/s41579-022-00807-9
7. Lee W-E, Park SW, Weinberger DM, Olson D, Simonsen L, Grenfell BT et al (2023) Direct and indirect mortality impacts of the COVID-19 pandemic in the United States, March 1, 2020 to January 1, 2022. Elife 12:e77562
8. World Health Organization (2021) "Infection prevention and control during health care when coronavirus disease ("COVID-19)" is suspected or confirmed: interim guidance, 12 July 2021. World Health Organization. https://apps.who.int/iris/handle/10665/342620

9. Laurie KL, Rockman S (2021) Which influenza viruses will emerge following the SARS-CoV-2 pandemic? Influenza Other Respir Viruses 15(5):573–576
10. Villani L, D'Ambrosio F, Ricciardi R, De Waure C, Calabrò GE (2022) Seasonal influenza in children: costs for the health system and society in Europe. Influenza Other Respir Viruses 16(5):820–831
11. Jiang L, Chen H, Li C (2023) Advances in deciphering the interactions between viral proteins of influenza a virus and host cellular proteins. Cell Insight 2(2):100079–100089
12. Forgione RE, Di Carluccio C, Kubota M, Manabe Y, Fukase K, Molinaro A et al (2020) Structural basis for glycan-receptor binding by mumps virus hemagglutinin-neuraminidase. Sci Rep 10(1):1589
13. Szczesniak I, Baliga-Gil A, Jarmolowicz A, Soszynska-Jozwiak M, Kierzek E (2023) Structural and functional RNA motifs of SARS-CoV-2 and Influenza A Virus as a target of viral inhibitors. Int J Mol Sci 24(2):1232
14. Shin W-J, Seong BL (2013) Recent advances in pharmacophore modeling and its application to anti-influenza drug discovery. Expert Opin Drug Discov 8(4):411–426
15. Fornells L, Couceiro J (2015) Resistance to FDA licensed anti-neuraminidase drugs used for Flu Treatment in the Americas: an overview of the incidence of resistant-strains of Seasonal and Pandemic Influenza Viruses from 2004 to 2014. Front Anti-Infective Drug Discovery 4:3–30
16. Neumann G, Kawaoka Y (2023) Which Virus Will Cause the Next Pandemic? Viruses 15(1):199
17. Abdullahi M, Shallangwa GA, Uzairu A (2020) In silico QSAR and molecular docking simulation of some novel aryl sulfonamide derivatives as inhibitors of H5N1 influenza a virus subtype. Beni-Suef Univ J Basic Appl Sci 9(1):1–12
18. Dorahy G, Chen JZ, Balle T (2023) Computer-aided Drug Design towards New Psychotropic and neurological drugs. Molecules 28(3):1324
19. Gan J-h, Liu J-x, Liu Y, Chen S-w, Dai W-t, Xiao Z-X et al (2022) DrugRep: an automatic virtual screening server for drug repurposing. Acta Pharmacol Sin. https://doi.org/10.1038/s41401-022-00996-2
20. Choudhury C, Murugan NA, Priyakumar UD (2022) Structure-based drug repurposing: traditional and advanced AI/ML-aided methods. Drug Discov Today. https://doi.org/10.1016/j.drudis.2022.03.006
21. Wu X, Xu LY, Li EM, Dong G (2022) Application of molecular dynamics simulation in biomedicine. Chem Biol Drug Des 99(5):789–800
22. Shi L, Yan F, Liu H (2023) Screening model of candidate drugs for breast cancer based on ensemble learning algorithm and molecular descriptor. Expert Syst Appl 213:119185
23. Li W, Xia L, Hu A, Liu A, Peng J, Tan W (2013) Design and synthesis of 4-A lkyl-2-amino (acetamino)-6-aryl-1, 3-thiazine derivatives as Influenza Neuraminidase inhibitors. Arch Pharm 346(9):635–644
24. Abdullahi M, Uzairu A, Shallangwa GA, Mamza PA, Ibrahim MT (2022) Computational modelling studies of some 1, 3-thiazine derivatives as anti-influenza inhibitors targeting H1N1 neuraminidase via 2D-QSAR, 3D-QSAR, molecular docking, and ADMET predictions. Beni-Suef Univ J Basic Appl Sci 11(1):1–22
25. Umar BA, Uzairu A, Shallangwa GA, Sani U (2019) QSAR modeling for the prediction of pGI50 activity of compounds on LOX IMVI cell line and ligand-based design of potent compounds using in silico virtual screening. Netw Model Anal Health Inf Bioinf 8(1):1–10
26. Abdullahi M, Adeniji SE, Arthur DE, Musa S (2020) Quantitative structure-activity relationship (QSAR) modelling study of some novel carboxamide series as new anti-tubercular agents. Bull Natl Res Centre 44(1):1–13
27. Mishra V, Kashyap S, Hasija Y (2015) Ligand based virtual screening for identifying potent inhibitors against viral neuraminidase: an in silico approach. J Taibah Univ Sci 9(1):20–26
28. Umar AB, Uzairu A, Shallangwa GA, Uba S (2020) Computational evaluation of potent 2-(1H-imidazol-2-yl) pyridine derivatives as potential V600E-BRAF inhibitors. Egypt J Med Hum Genet 21(1):67
29. Abdullahi M, Uzairu A, Shallangwa GA, Arthur DE, Umar BA, Ibrahim MT (2020) Virtual molecular docking study of some novel carboxamide series as new anti-tubercular agents. Eur J Chem 11(1):30–36
30. Takashita E, Fujisaki S, Kishida N, Xu H, Imai M, Tashiro M et al (2013) Characterization of neuraminidase inhibitor-resistant influenza A(H1N1)pdm09 viruses isolated in four seasons during pandemic and post-pandemic periods in Japan. Influenza Other Respir Viruses 7(6):1390–1399
31. Beard K, Brendish N (2018) Clark T Treatment of influenza with neuraminidase inhibitors. Current Opin Infecti. https://doi.org/10.1097/QCO.0000000000000496
32. Arthur DE, Samuel AN, Ejeh S, Adeniji SE, Adedirin O, Abdullahi M (2020) Computational study of some cancer drugs as potent inhibitors of GSK3β. Sci Afr 10:e00612
33. Uniyal A, Mahapatra MK, Tiwari V, Sandhir R, Kumar R (2022) Targeting SARS-CoV-2 main protease: structure based virtual screening, in silico ADMET studies and molecular dynamics simulation for identification of potential inhibitors. J Biomol Struct Dynamics 40(8):3609–3625
34. Radwan HA, Ahmad I, Othman IM, Gad-Elkareem MA, Patel H, Aouadi K et al (2022) Design, synthesis, in vitro anticancer and antimicrobial evaluation, SAR analysis, molecular docking and dynamic simulation of new pyrazoles, triazoles and pyridazines based isoxazole. J Mol Struc 1264:133312.
35. Ahmad I, Pawara R, Patel H (2022) In silico toxicity investigation of Methaqualone's conjunctival, retinal, and gastrointestinal hemorrhage by molecular modelling approach. Mol Simul. https://doi.org/10.1080/08927022.2022.2113412
36. Chaudhari B, Patel H, Thakar S, Ahmad I, Bansode D (2022) Optimizing the Sunitinib for cardio-toxicity and thyro-toxicity by scaffold hopping approach. Silico Pharmacol 10(1):1–14
37. Farhan MM, Guma MA, Rabeea MA, Ahmad I, Patel H (2022) Synthesizes, characterization, molecular docking and in vitro bioactivity study of new compounds containing triple beta lactam rings. J Mol Struct 1269:133781
38. Osmaniye D, Karaca Ş, Kurban B, Baysal M, Ahmad I, Patel H et al (2022) Design, synthesis, molecular docking and molecular dynamics studies of novel triazolothiadiazine derivatives containing furan or thiophene rings as anticancer agents. Bioorg Chem 122:105709
39. Desai NC, Joshi SB, Khasiya AG, Jadeja DJ, Mehta HK, Pandya M et al (2022) Pyrazolo-imidazolidinones: synthesis, antimicrobial assessment and molecular modelling studies by molecular mechanic and quantum mechanic approach. J Mol Struct 1270:134000
40. Paul RK, Ahmad I, Patel H, Kumar V, Raza K (2022) Phytochemicals from Amberboa ramosa as potential DPP-IV inhibitors for the management of Type-II diabetes Mellitus: inferences from In-silico investigations. J Mol Struct 1271: 134045.
41. Murugesan S, Ragavendran C, Ali A, Arumugam V, Lakshmanan DK, Palanichamy P et al (2023) Screening and druggability analysis of Marine active metabolites against SARS-CoV-2: an Integrative Computational Approach. Int J Translational Med 3(1):27–41
42. Umar AB, Uzairu A (2023) Virtual screening, pharmacokinetic, and DFT studies of anticancer compounds as

potential V600E-BRAF kinase inhibitors. J Taibah Univ Med Sci 18(5):933–946
43. Reeda VJ, Jothy VB (2023) Vibrational spectroscopic, quantum computational (DFT), reactivity (ELF, LOL and Fukui), molecular docking studies and molecular dynamic simulation on (6-methoxy-2-oxo-2H-chromen-4-yl) methyl morpholine-4-carbodithioate. J Mol Liq 371:121147
44. Liu Y, Zhang L, Gong J, Fang H, Liu A, Du G et al (2011) Design, synthesis, and biological activity of thiazole derivatives as novel influenza neuraminidase inhibitors. J Enzyme Inhib Med Chem 26(4):506–513
45. Ourdjini Z, Kraim K, Winum J-Y, Benoist E, Seridi A (2023) A combined DFT and molecular docking study on novel tricarbonylrhenium (I) complexes bearing mono-and bivalent benzenesulfonamide scaffolds as human carbonic anhydrase IX and XII inhibitors. J Mol Struct 1282:135211
46. Acar Çevik U, Celik I, Işık A, Ahmad I, Patel H, Özkay Y et al (2022) Design, synthesis, molecular modeling, DFT, ADME and biological evaluation studies of some new 1, 3, 4-oxadiazole linked benzimidazoles as anticancer agents and aromatase inhibitors. J Biomol Struct Dyn. https://doi.org/10.1080/07391102.2022.2025906
47. Boulaamane Y, Ahmad I, Patel H, Das N, Britel MR, Maurady A (2022) Structural exploration of selected C6 and C7-substituted coumarin isomers as selective MAO-B inhibitors. J Biomol Struct Dyn. https://doi.org/10.1080/07391102.2022.2033643
48. Vickers NJ (2017) Animal communication: when i'm calling you, will you answer too? Curr Biol 27(14):R713–R5
49. Abdelgawad MA, Oh JM, Parambi DGT, Kumar S, Musa A, Ghoneim MM et al (2022) Development of bromo- and fluoro-based α, β-unsaturated ketones as highly potent MAO-B inhibitors for the treatment of Parkinson's disease. J Mol Struct 1266:133545
50. Tople MS, Patel NB, Patel PP, Purohit AC, Ahmad I, Patel H (2022) An in silico-in vitro antimalarial and antimicrobial investigation of newer 7-Chloroquinoline based Schiff-bases. J Mol Struct 1271: 134016.
51. Baammi S, Daoud R, El Allali A (2023) In silico protein engineering shows that novel mutations affecting NAD + binding sites may improve phosphite dehydrogenase stability and activity. Sci Rep 13(1):1878
52. Abdullahi M, Uzairu A, Shallangwa GA, Mamza PA, Ibrahim MT (2022) 2D-QSAR, 3D-QSAR, molecular docking and ADMET prediction studies of some novel 2-((1H-indol-3-yl)thio)-N-phenyl-acetamide derivatives as anti-influenza a virus. Egypt J Basic Appl Sci 9(1):510–532
53. Karami TK, Hailu S, Feng S, Graham R, Gukasyan HJ (2022) Eyes on Lipinski's rule of five: a new "Rule of Thumb" for Physicochemical Design Space of Ophthalmic Drugs. J Ocul Pharmacol Ther 38(1):43–55
54. Chauhan K, Singh P, Kumar V, Shukla PK, Siddiqi MI, Chauhan PM (2014) Investigation of Ugi-4CC derived 1H-tetrazol-5-yl-(aryl) methyl piperazinyl-6-fluoro-4-oxo-1,4-dihydroquinoline-3-carboxylic acid: synthesis, biology and 3D-QSAR analysis. Eur J Med Chem 78:442–454
55. Ahmed A, Saeed A, Ejaz SA, Aziz M, Hashmi MZ, Channar PA et al (2022) Novel adamantyl clubbed iminothiazolidinones as promising elastase inhibitors: design, synthesis, molecular docking, ADMET and DFT studies. RSC Adv 12(19):11974–11991
56. Hadni H, Bakhouch M, Elhallaoui M (2021) 3D-QSAR, molecular docking, DFT and ADMET studies on quinazoline derivatives to explore novel DHFR inhibitors. J Biomol Struct Dyn. https://doi.org/10.1080/07391102.2021.2004233
57. ElMchichi L, Belhassan A, Lakhlifi T, Bouachrine M (2020) 3D-QSAR study of the chalcone derivatives as anticancer agents. J Chem. https://doi.org/10.1155/2020/5268985
58. Li H, Sheng Y, Li W, Yuan L (2022) Recent advances in molecular fluorescent probes for CYP450 sensing and imaging. Chemosensors 10(8):304
59. Kraithong S, Teerapattarakan N, Balasubramanian B, Issara U (2022) Bioactive compounds in tea: Effect of imbalanced intake on digestive enzymes activity, cytochrome inhibition and drug interaction. South Afr J Bot 150:58–68
60. Adekoya OC, Adekoya GJ, Sadiku ER, Hamam Y, Ray SS (2022) Application of DFT calculations in designing polymer-based drug delivery systems: an overview. Pharmaceutics 14(9):1972
61. Taghour MS, Elkady H, Eldehna WM, El-Deeb N, Kenawy AM, Elkaeed EB et al (2022) Design, synthesis, anti-proliferative evaluation, docking, and MD simulations studies of new thiazolidine-2, 4-diones targeting VEGFR-2 and apoptosis pathway. PLoS ONE 17(9):e0272362
62. Alghamdi SK, Abbas F, Hussein RK, Alhamzani AG, El-Shamy NT (2023) Spectroscopic characterization (IR, UV-Vis), and HOMO-LUMO, MEP, NLO, NBO analysis and the antifungal activity for 4-Bromo-N-(2-nitrophenyl) benzamide; using DFT modeling and in silico molecular docking. J Mol Struct 1271:134001
63. Khalid M, Shafiq I, Mahmood K, Hussain R, ur Rehman MF, Assiri MA et al (2023) Effect of different end-capped donor moieties on non-fullerenes based non-covalently fused-ring derivatives for achieving high-performance NLO properties. Sci Rep 13(1):1395
64. Hussein HA, Fadhil GF (2023) Theoretical investigation of para amino-dichloro chalcone isomers. Part II: a DFT structure–stability study of the FMO and NLO Properties. ACS Omega 8(5):4937-4953
65. Mohammadi M, Hoseinpour F, Khanmohammadi A (2022) A DFT theoretical investigation on the interplay effects between cation-π and intramolecular hydrogen bond interactions in the mesalazine··· Fe2 + binary complex. Theor Chem Acc 141(8):1–12
66. Chaudhary T, Chaudhary MK, Joshi BD (2021) Topological and reactivity descriptor of carisoprodol from DFT and molecular docking approach. J Inst Sci Technol 26(1):74–82
67. Pal R, Chattaraj PK (2021) Chemical reactivity from a conceptual density functional theory perspective. J Indian Chem Soc 98(1):100008
68. Janani S, Rajagopal H, Muthu S, Aayisha S, Raja M (2021) Molecular structure, spectroscopic (FT-IR, FT-Raman, NMR), HOMO-LUMO, chemical reactivity, AIM, ELF, LOL and molecular docking studies on 1-Benzyl-4-(N-Boc-amino) piperidine. J Mol Struct 1230:129657
69. Abd Emoniem N, Mukhtar R, Ghaboosh H, Elshamly E, Mohamed M, Elsaman T et al (2023) Turning down PI3K/AKT/mTOR signalling pathway by natural products: an in silico multi-target approach. SAR QSAR Environ Res 34(2):163–182